Hindawi
Journal of Chemistry
Volume 2017, Article ID 2871034, 14 pages
https://doi.org/10.1155/2017/2871034

Research Article

Fatty Amides from Crude Rice Bran Oil as Green Corrosion Inhibitors

E. Reyes-Dorantes,[1,2] J. Zuñiga-Díaz,[1,2] A. Quinto-Hernandez,[1] J. Porcayo-Calderon,[2,3] J. G. Gonzalez-Rodriguez,[3] and L. Martinez-Gomez[2,4]

[1] *Tecnológico Nacional de México, Instituto Tecnológico de Zacatepec, Calzada Instituto Tecnológico 27, 62780 Zacatepec, MOR, Mexico*
[2] *Instituto de Ciencias Físicas, Universidad Nacional Autónoma de México, Avenida Universidad, s/n, 62210 Cuernavaca, MOR, Mexico*
[3] *CIICAp, Universidad Autónoma del Estado de Morelos, Avenida Universidad 1001, 62209 Cuernavaca, MOR, Mexico*
[4] *Corrosion y Protección (CyP), Buffon 46, 11590 Mexico City, Mexico*

Correspondence should be addressed to J. Porcayo-Calderon; jporcayoc@gmail.com

Received 1 February 2017; Revised 27 March 2017; Accepted 5 April 2017; Published 18 May 2017

Academic Editor: Hassan Arida

Due to its high oil content, this research proposes the use of an agroindustrial byproduct (rice bran) as a sustainable option for the synthesis of corrosion inhibitors. From the crude rice bran oil, the synthesis of fatty amide-type corrosion inhibitors was carried out. The corrosion inhibitory capacity of the fatty amides was evaluated on an API X-70 steel using electrochemical techniques such as real-time corrosion monitoring and potentiodynamic polarization curves. As a corrosive medium, a CO_2-saturated solution (3.5% NaCl) was used at three temperatures (30, 50, and 70°C) and different concentrations of inhibitor (0, 5, 10, 25, 50, and 100 ppm). The results demonstrate that the sustainable use of agroindustrial byproducts is a good alternative to the synthesis of environmentally friendly inhibitors with high corrosion inhibition efficiencies.

1. Introduction

Corrosion is the degradation process of a material due to its exposure to the environment, and is one of the major problems affecting its performance, safety, and integrity. Despite the continuous advances in the field of materials with corrosion resistance, the use of corrosion inhibitors is one of the most practical and economical ways to control it [1, 2]. An inhibitor is defined as any chemical which, when added in small concentrations to an aggressive environment, significantly reduces the corrosion rate of the material in contact with the corrosive environment. A wide variety of organic and inorganic compounds have been used to control corrosion. It has been demonstrated that many organic molecules can act as corrosion inhibitors because of their affinity with the metal surfaces, replacing the adsorbed water molecules and thereby forming a molecular film that prevents the metal dissolution. In the particular case of environments where the presence of hydrocarbons predominates, the inhibitors based on amide- or imidazolines-type compounds are widely used [3–9]. The excellent performance of this type of corrosion inhibitors is associated with the fact that its molecules are constituted by two essential parts: an electron-rich polar part capable of adhering onto a metal surface through coordination bonds and a hydrophobic part which can effectively prevent the diffusion of contaminants present in the aggressive environment [2, 5, 9–12]. In addition to the above, it has also been reported that the presence of unsaturation or other functional groups of the alkyl chains also influences their inhibition efficacy [7, 9, 13]. These characteristics are provided by the nature of the vegetable oil used for the synthesis of this type of inhibitors.

From the point of view of sustainable development, it is imperative to search for new alternative nonconventional

sources of vegetable oils. These new sources of vegetable oils can be used for applications as diverse as biofuels synthesis, biopolymers, corrosion inhibitors, and so forth [6, 9, 14, 15]. In this sense, rice bran is a byproduct of the rice grain milling process. In general, the overall yield of the rice milling process is about 60% white rice, 10% broken grains, 10% bran, and 20% husks [16]. The rice bran is the main oil source of the rice grain, in addition to a good content of proteins, tocopherols, and bioactive compounds. Its oil content varies from 10 to 23%, and its fatty acids are 47% monounsaturated, 33% polyunsaturated, and 20% saturated, in addition to a significant fraction of unsaponifiable components (4.3%) [17, 18]. However, only 10% of the world's rice bran production is used for oil extraction, and the remainder is used as a low-cost feed for cattle and poultry. The high oil content of the rice bran combined with the presence of the lipase enzyme causes that this byproduct has a short shelf life due to the degradation of its oil [16–18].

Therefore, the aim of this work is to explore the use of a sustainable source for the synthesis of corrosion inhibitors, where the source of vegetable oil is environmentally friendly by not affecting the food chain, does not replace crops, and does not use new crop fields for their production. The amide-type inhibitors synthesized were evaluated by two types of experimental measurements: real-time corrosion monitoring and potentiodynamic polarization curves. The corrosive medium used was a CO_2-saturated sodium chloride solution at different temperatures.

2. Experimental Procedure

2.1. Synthesis of Fatty Amides from Crude Rice Bran Oil. The rice bran was obtained from a local mill (Puente de Ixtla, Morelos, Mexico). Rice bran was collected a few hours after its production. Crude rice bran oil (CRBO) content was determined by the Soxhlet method, where the solvent used was hexane. The extraction of the CRBO used for the synthesis process was carried out in a stirred batch system at room temperature, using a rice bran to solvent ratio of 1 : 10. Chemical and physicochemical characterization of the CRBO was made.

The method used for the synthesis of the fatty amides is a modification to the procedure suggested by Kumar et al. [19]. In general, the procedure consists of introducing one mole of crude oil with 3 moles of aminoethylethanolamine (AEEA) into the reactor (1 : 3 CRBO-AEEA ratio). The mixture is heated to 140°C with stirring at atmospheric pressure. Once the temperature is reached, the course of the reaction is monitored by thin-film chromatography (TLC), until the triglycerides disappear completely.

2.2. Electrochemical Evaluation of Fatty Amides as Corrosion Inhibitors. The evaluation of the electrochemical performance of the synthesized compounds was performed on an API X-70 steel, commonly used in the manufacture of pipelines for the transportation of hydrocarbons. The performance of the inhibitors was evaluated by two types of electrochemical techniques, namely, real-time corrosion measurements and potentiodynamic polarization curves.

Real-time corrosion measurements were performed using an identical three-electrode probe. Steel samples with dimensions of $0.3 * 1.0 * 1.0$ cm were cut, and a conductive wire was spot-welded on one of its narrow sides. For the electrochemical tests, three steel samples were encapsulated in acrylic resin with a separation between them of 1 mm. Each encapsulation was abraded with silicon carbide abrasive paper from 120 to 600 grids; then the encapsulations were washed with alcohol and distilled water, dried, and immediately employed in the electrochemical tests. A solution of NaCl (3.5% by weight) saturated with CO_2 was used as the corrosive medium. The solution was saturated with CO_2 two hours prior to the tests and the CO_2 bubbling was maintained during the corrosion tests. Corrosion tests were for 24 hours, at a test temperature of 30, 50, and 70°C, with light stirring. Encapsulations were kept inside the electrolyte for one hour before any inhibitor was added. The concentrations of inhibitor evaluated were 0, 5, 10, 25, 50, and 100 ppm. For each electrochemical test, a volume of 400 mL of electrolyte was used. The multitechnique electrochemical monitoring equipment (SmartCET) is based on a combination of electrochemical techniques such as electrochemical noise (EN), linear polarization resistance (LPR), and harmonic distortion analysis (HDA), and as a result of this interrelationship, both the corrosion rate and the pitting corrosion behavior of the material under study are obtained. The measurement cycle is carried out for a period of 430 seconds as follows: measurements of EN in current and potential, second to second for 300 seconds, LPR/HDA measurements for 100 seconds, and electrolyte resistance measurement for 30 seconds. The details of this real-time monitoring technique are described in the scientific literature [20, 21].

For potentiodynamic polarization curves, a typical three-electrode arrangement was used where the reference electrode was a Pt wire and as counterelectrode a high-purity graphite rod was used. From this type of tests, it is possible to determine the electrochemical parameters such as corrosion potential and corrosion rate, in addition to the anodic and cathodic slopes from the extrapolation of the Tafel slopes of the obtained curves. In this case, steel samples with a reaction area of 1 cm^2 were encapsulated in acrylic resin. Encapsulations were abraded with silicon carbide abrasive paper from 120 to 600 grids; after that, they were washed with alcohol and distilled water, dried, and immediately employed in the electrochemical test. Corrosive conditions were the same as those of real-time corrosion measurements. In order to ensure that the inhibitor achieved the maximum surface coverage of the working electrode, before starting the assay, samples were allowed to stabilize for 24 hours into electrolyte prior to performing the assay. Potentiodynamic polarization tests were performed from −400 mV to 600 mV with respect to open circuit potential (E_{corr}) at a sweep rate of 1 mV/s. Electrochemical parameters were calculated using the extrapolation Tafel method considering an extrapolation potential of ±250 mV around the value of the corrosion potential. Potentiodynamic polarization curves were carried out using an ACM Instruments zero-resistance ammeter (ZRA) coupled to a personal computer.

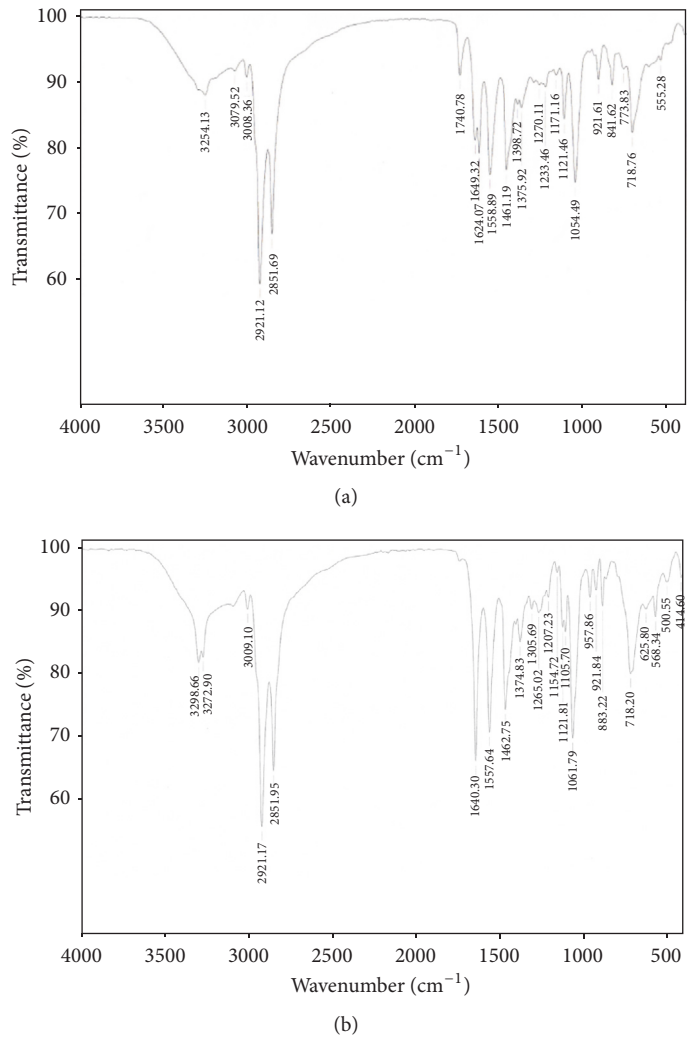

Figure 1: FT-IR spectra of the synthesis of the fatty amides from CRBO and AEEA: (a) initial mixture (t = 0 minutes reaction) and (b) final mixture (80 minutes reaction).

3. Results and Discussion

3.1. Synthesis of Fatty Amides. Rice bran analysis indicated a crude oil content of 21% (dry basis), which is in agreement with data reported in the literature [16–18]. Its molecular weight calculated from its saponification index was 923.36, and its chemical characterization showed an oleic acid content of 48.48%, 35.26% of linoleic acid, and 14.54% of palmitic acid, similar values to those reported in the literature for this type of oil [16, 17]. Knowledge of the type of fatty acids present in the oil is important, given that both the length and unsaturation of the hydrocarbon chain contribute to the mode of adsorption and inhibition efficiency of the inhibitor molecule [7].

Figure 1 shows the FT-IR spectra of the fatty amides synthesized from CRBO and AEEA. From Figure 1, it can be seen that the signal at 1740 cm^{-1} corresponding to the C=O stretching of the triglycerides disappears, and a new signal is observed at 1640 cm^{-1}. It is known that the presence of this signal is characteristic of the peaks corresponding to the amidation product (fatty amides) [10–19]. Evolution of the FT-IR spectra at different times (spectra not shown) indicated that, after 80 minutes of reaction, the complete disappearance of the triglycerides was achieved, suggesting formation of fatty amides.

3.2. Real-Time Corrosion Measurements of Synthesized Fatty Amides. Figure 2 shows the effect of the inhibitor addition (fatty amide) on the corrosion rate (based on RPL measurements) of API X-70 steel immersed in CO_2-saturated saline solution at different test temperatures. In all cases, the inhibitor was added 60 minutes after the measurements were started. RPL measurement involves measuring the polarization resistance (Rp) using a sinusoidal polarization of small amplitude (±20 mV) of the working electrode (steel under study). In this case, the slope of the potential-current sweep is Rp, which is inversely proportional to the corrosion current density, and it is subsequently transformed to corrosion rate.

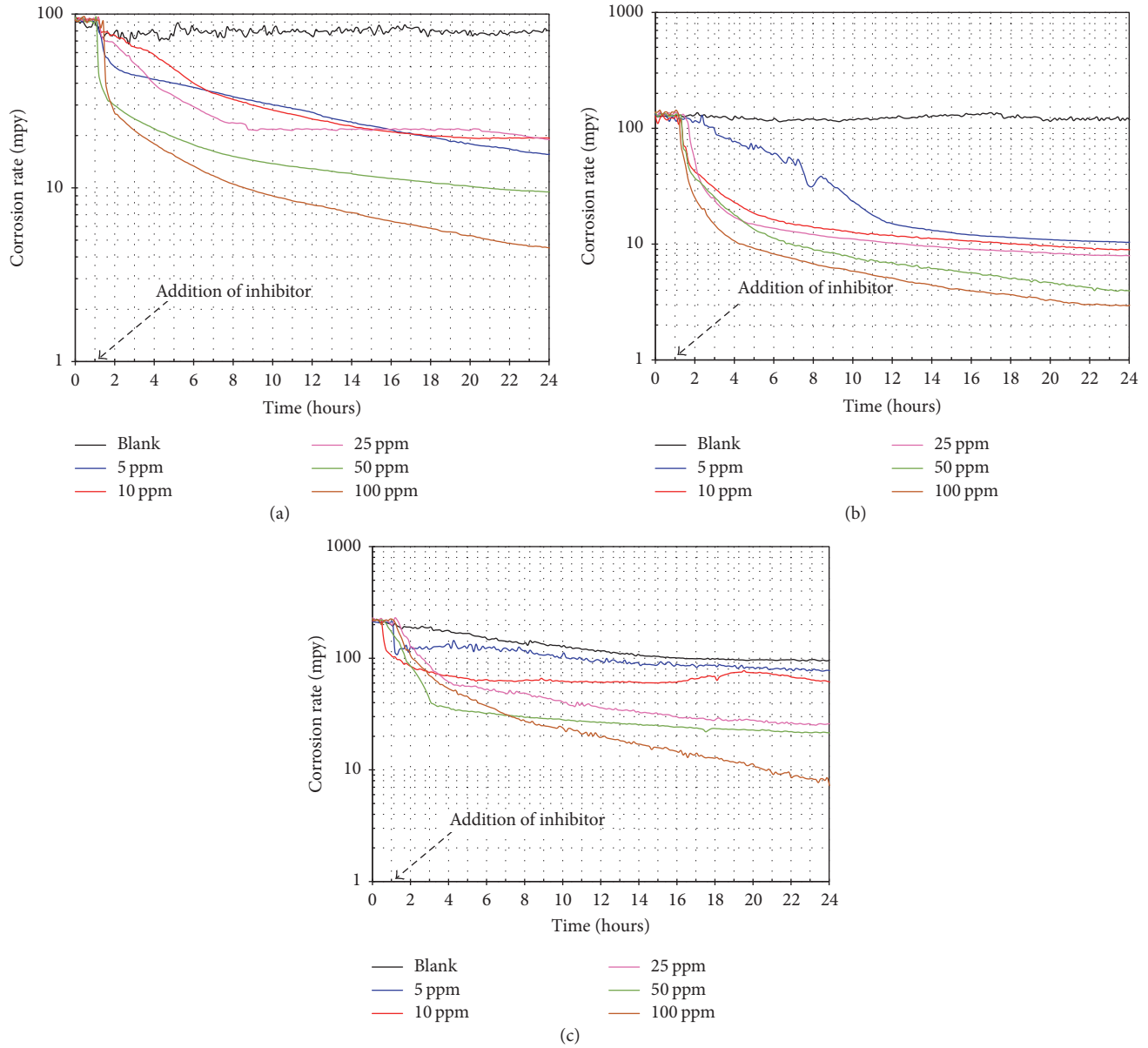

FIGURE 2: Variation of corrosion rate determined by RPL (real-time monitoring) versus time for API X-70 steel exposed to 3.5% NaCl solution saturated with CO_2 at different concentrations of fatty amide: (a) 30°C, (b) 50°C, and (c) 70°C.

It is observed that in the absence of inhibitor the corrosion rate of API X-70 steel is higher regardless of temperature. Only at 70°C, it is observed that this tends to decrease markedly as a function of time. This may be due to precipitation of $FeCO_3$ crystals onto steel surface. In general, this behavior is due to the electrochemical nature of the corrosion process of carbon steel, where both the anodic iron dissolution and the cathodic evolution of hydrogen take place [22]. The protection process (iron carbonate precipitation) is due to the CO_2 hydration which causes the formation of carbonic acid:

$$CO_2 + H_2O \longrightarrow H_2CO_3 \quad (1)$$

Since the electrolyte is deaerated, the possible dominant cathodic reactions can be H^+ ions reduction, water reduction, and the carbonic acid dissociation:

$$2H^+ + 2e^- \longrightarrow H_2 \quad (2)$$

$$2H_2O + 2e^- \longrightarrow 2OH^- + H_2 \quad (3)$$

$$H_2CO_2 + e^- \longrightarrow H^+ + HCO_3^- \quad (4)$$

$$HCO_3^- + e^- \longrightarrow H^+ + CO_3^{-2} \quad (5)$$

And, the primary anodic reaction is the dissolution of iron:

$$Fe \longrightarrow Fe^{+2} + 2e^- \quad (6)$$

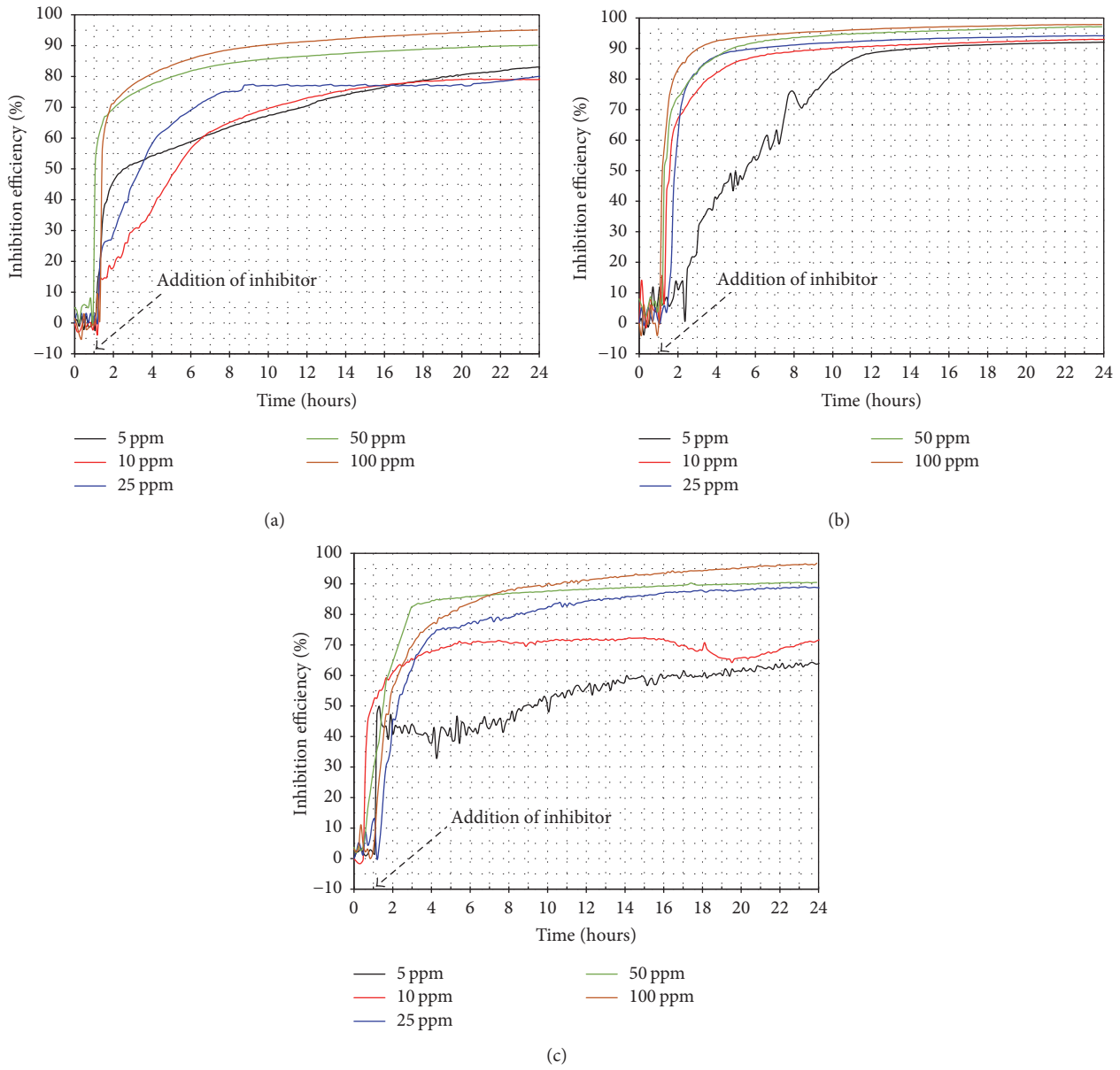

FIGURE 3: Variation of the inhibition efficiency determined from RPL measurements (real-time monitoring): (a) 30°C, (b) 50°C, and (c) 70°C.

During the steel corrosion process, the iron carbonate precipitation onto steel surface is possible, according to

$$Fe^{+2} + CO_3{}^{-2} \longrightarrow FeCO_3 \quad (7)$$

$FeCO_3$ precipitation modifies the corrosion process kinetics, because a physical porous barrier is formed between the electrolyte and metal surface. This barrier influences the transport of the corrosive species of the electrolyte. However, the protection of this porous layer depends on several environmental conditions, such as iron concentration, pH solution, temperature, CO_2 partial pressure, mechanical forces due to flow conditions, and steel microstructure [23]. Due to the imperfect nature of this protective scale (cracks and porosity), the electrolyte can permeate to the metal surface and corrode the steel causing the detachment of the protective scale [24]. Therefore, the protection provided by the precipitation of iron carbonate is limited.

On the other hand, in the inhibitor's presence, the corrosion rate decreases as its concentration increases, regardless of the test temperature. At the maximum concentration of inhibitor, a reduction of one order of magnitude in the corrosion rate is observed. In all cases, a drastic drop in the corrosion rate values is observed in the first 3-4 hours after the inhibitor has been added; subsequently, the corrosion rate tends to decrease slowly without reaching a defined steady state. This reduction in the corrosion rate is due to the adsorption of an inhibitor film onto steel surface which acts as a more effective barrier to permeation of the corrosive electrolyte towards the metal surface. The effectiveness of an

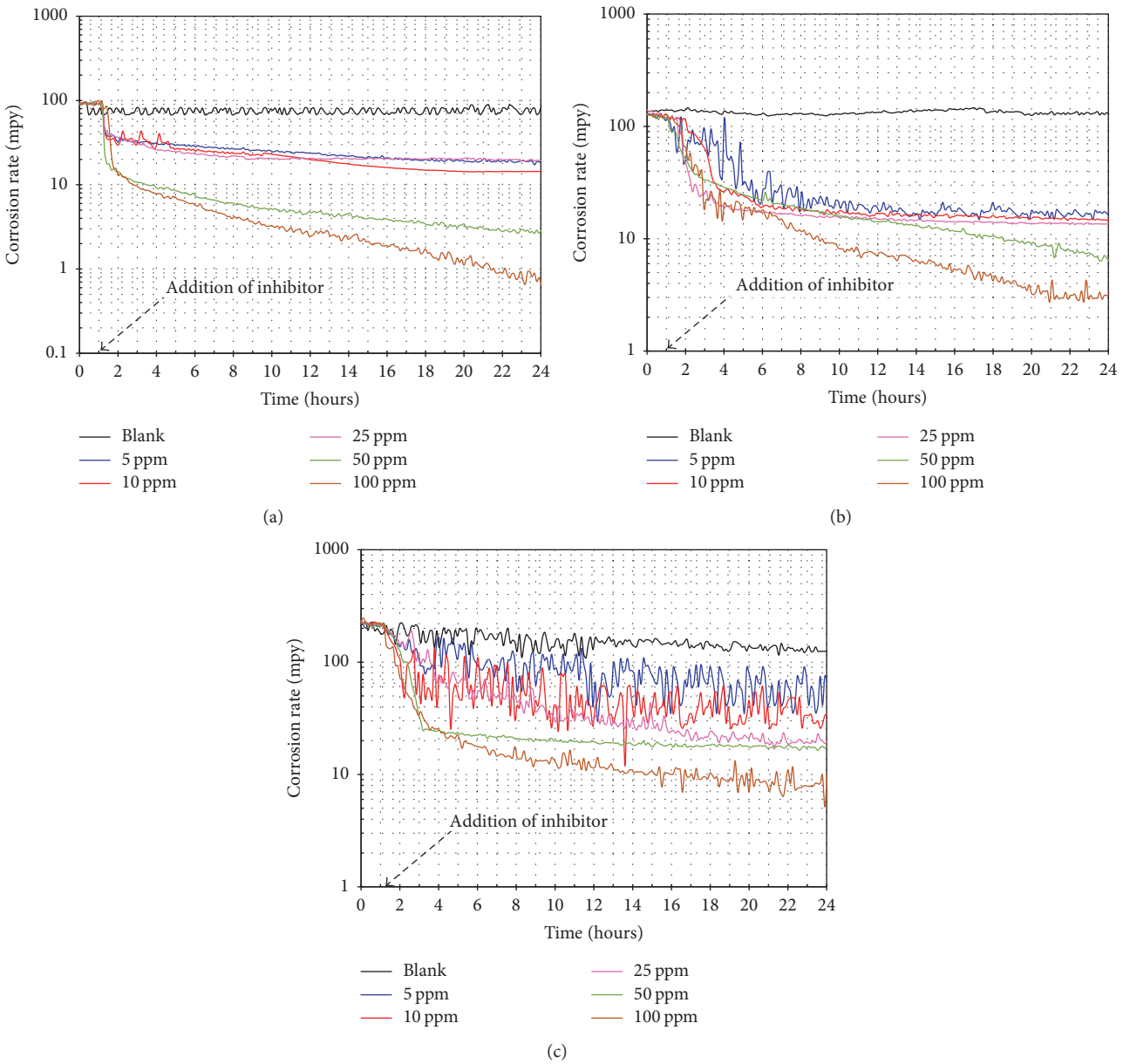

FIGURE 4: Variation of corrosion rate as determined by HDA (real-time monitoring) versus time for API X-70 steel exposed to CO_2-saturated saline solution at different inhibitor concentration: (a) 30°C, (b) 50°C, and (c) 70°C.

inhibitor of organic nature is the result of the physicochemical properties of the molecule, the nature of its functional groups, possible steric effects, and the electron density of the donor atoms [9]. Inhibitor adsorption depends on the interaction of the π orbitals of the inhibitor molecule with the orbitals of the atoms of the metal surface [9].

Figure 3 shows the variation of the inhibition efficiency of fatty amides as a function of time (from the RPL measurements of Figure 2). The inhibition efficiency was determined according to the following relation:

$$E\,(\%) = \frac{\mathrm{CR}_i - \mathrm{CR}_b}{\mathrm{CR}_i} * 100, \tag{8}$$

where CR_b is the corrosion rate in inhibitor absence and CR_i when the inhibitor is present. In all cases, the inhibition efficiency increased with the added inhibitor concentration, regardless of test temperature. The inhibition efficiency was greater than 95% at the maximum inhibitor concentration evaluated, and, in all cases, the steady state was not reached. This implies that, in longer periods of exposure, the inhibition efficiency would tend to increase.

Figure 4 shows the variation in the corrosion rate, determined from the HDA measurements, as a function of time for the API X-70 steel exposed in CO_2-saturated saline solution at 30, 50, and 70°C at different concentrations of inhibitor. The analysis of harmonics and the nonlinear response are based on the disturbance of an AC signal and the

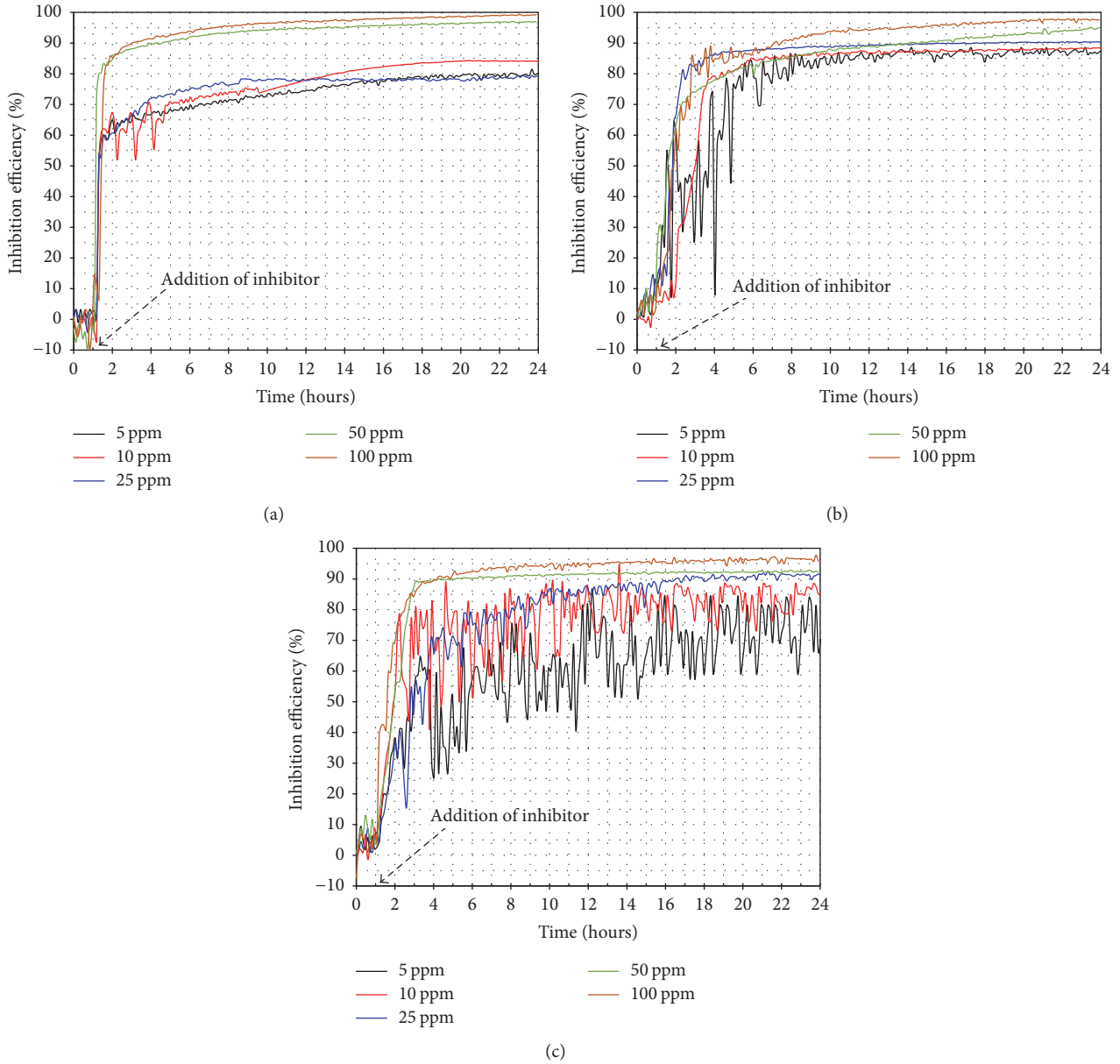

Figure 5: Variation of inhibition efficiency determined from HDA-based measurements (real-time monitoring): (a) 30°C, (b) 50°C, and (c) 70°C.

frequency domain, correspondingly. The latter is a measure of the nonlinear current distortion, originated during the RPL measurement, using a 10 mHz sine wave (50 mV peak-to-peak), and analyzes current signals at 10, 20, and 30 mHz. This allows obtaining the kinetic parameters of the corrosion process. The harmonics analysis in the current response offers the possibility of obtaining the corrosion rate and the anodic and cathodic parameters of Tafel.

In general, the corrosion rates obtained from the HDA-based measurements suggest a similar trend to those obtained from the RPL measurements. The possible differences observed are due to the fact that, for the calculation of the corrosion rate, the HDA technique uses instantaneous values of the anodic and cathodic Tafel slopes and, in RPL-based measurements (Figure 2), the technique uses fixed values (120 mV). Observation of disturbances in the measurements is notorious, and their magnitude increases with the temperature and even more when the inhibitor is present. Since such perturbations can be interpreted as adsorption-desorption processes of the inhibitor molecules and these processes promote the presence of active sites onto metal surface, both corrosion potential values (E_{corr}) and Tafel kinetic parameters can be affected [7].

Thus, the calculation of the corrosion rate to use instantaneous Tafel values is advisable. Employing constant values will show a smoothed trend which suppresses the transient processes. In this sense, it can be observed that the amplitude of the transients increases with the temperature and, for

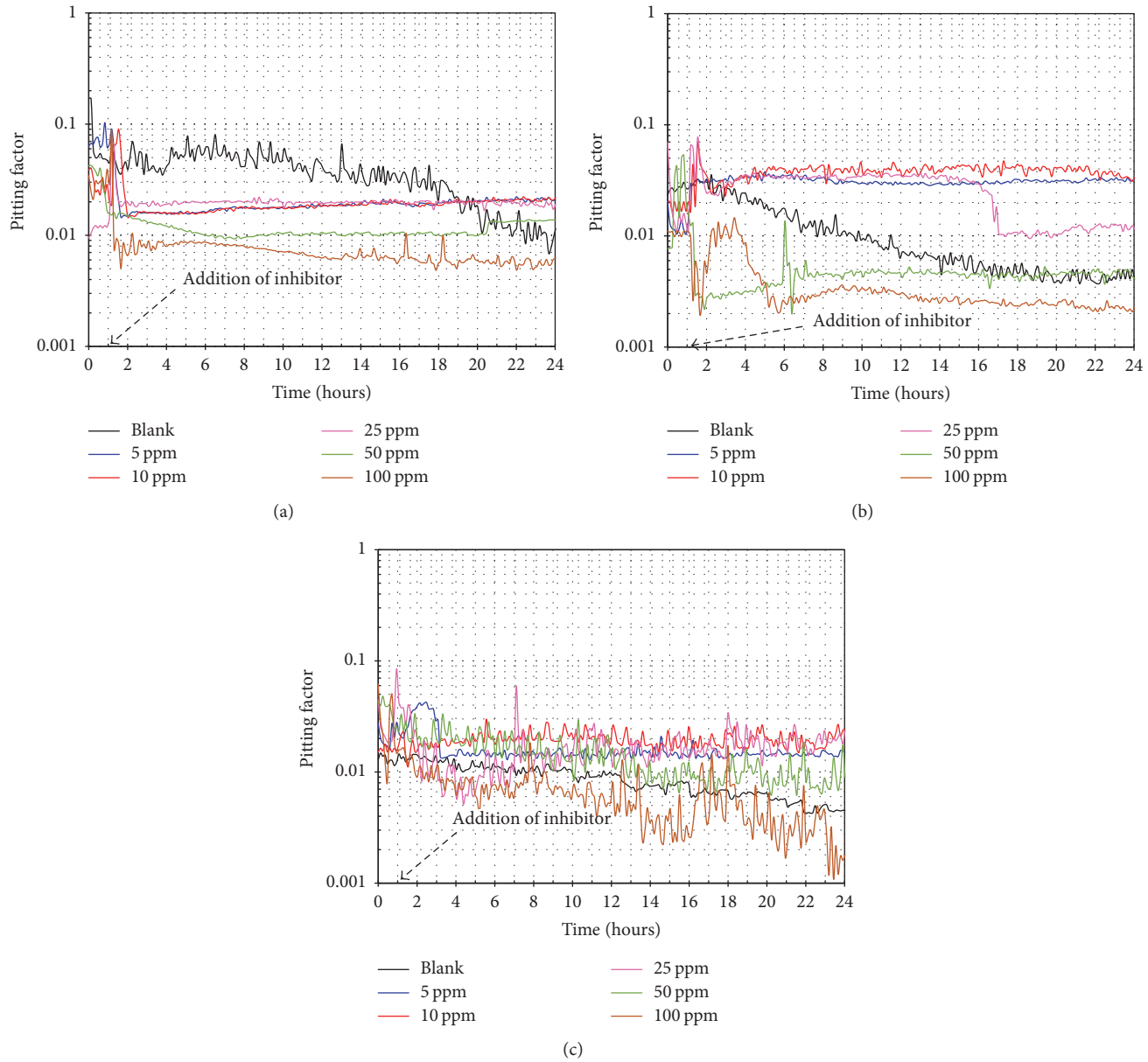

Figure 6: Variation in PF values as a function of time for API X-70 steel exposed to CO_2-saturated saline solution at different inhibitor concentrations: (a) 30°C, (b) 50°C, and (c) 70°C.

a given temperature, decreases with the inhibitor concentration. This suggests two facts: (1) the inhibitor molecules adsorption can be compromised by increasing temperature and (2) when the inhibitor concentration is increased, there are a greater number of molecules occupying the active sites left by the desorption of the inhibitor molecules.

Similarly, the evolution of the inhibition efficiency from the HDA-based corrosion rate measurements (Figure 4) is shown in Figure 5. As indicated, the observed transients can be interpreted as a measure of the adsorption stability of the inhibitor molecules onto metal surface. Mainly, increasing the inhibitor concentration decreases both the amplitude and frequency of the instabilities.

Figure 6 shows the variation of pitting factor (PF) as a function of time for API X-70 steel exposed to CO_2-saturated saline solution at different test temperatures, with and without inhibitor addition. This parameter is obtained from EN and HDA measurements, where EN refers to current and potential fluctuations that occur onto steel surface without disturbance of its potential. EN measurements provide information on the activity level of the corrosion process and the dominant corrosion mechanism. The pitting factor is defined as follows [25]:

$$\mathrm{PF} = \frac{\sigma I_{\mathrm{EN}}}{A_{\mathrm{WE}} I_{\mathrm{HA}}}, \tag{9}$$

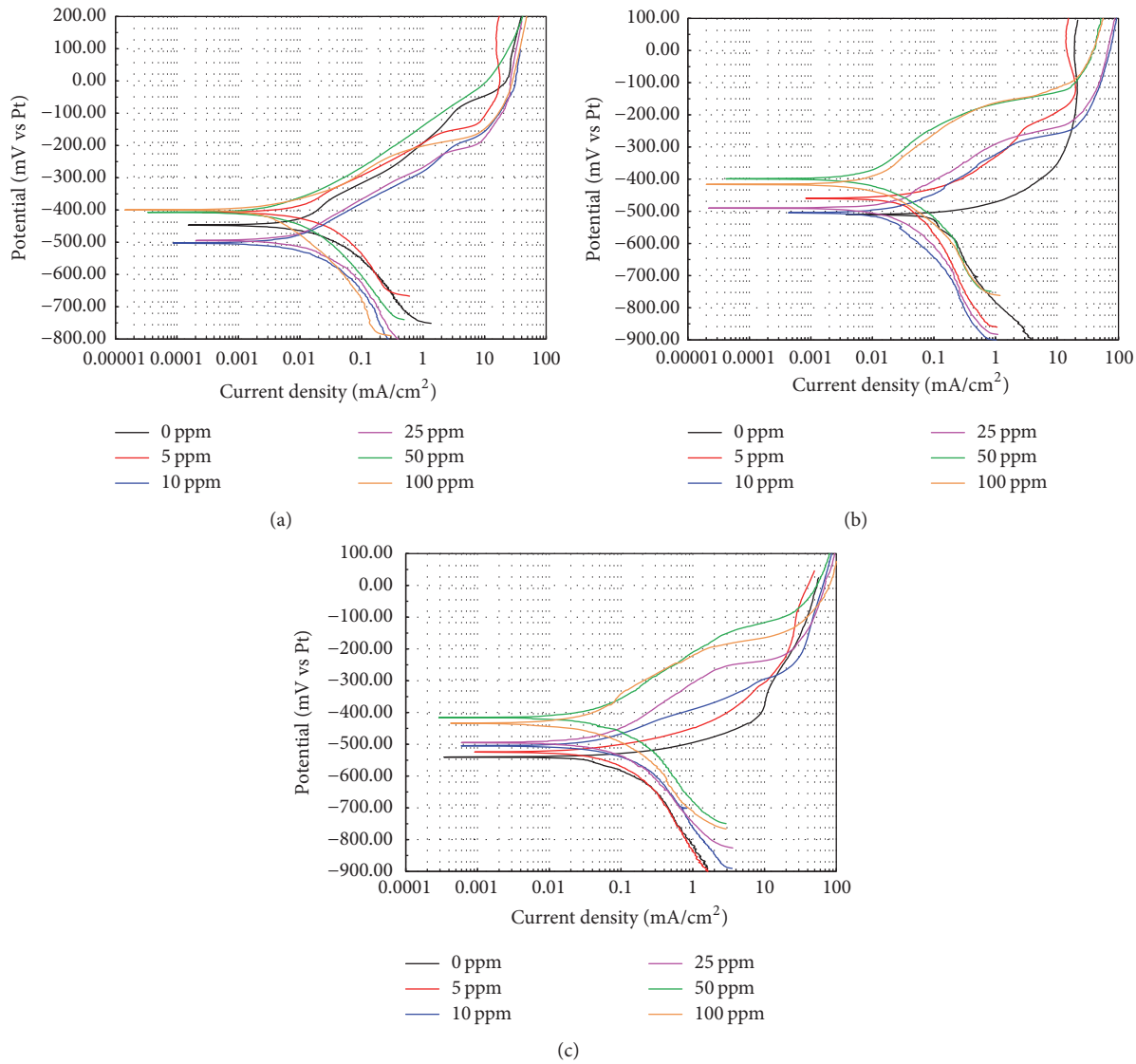

FIGURE 7: Potentiodynamic polarization curves for API X-70 steel in CO_2-saturated saline solution at different concentrations of inhibitor: (a) 30°C, (b) 50°C, and (c) 70°C, after 24 hours of stabilization.

where σI_{EN} is the standard deviation of the current (determined by electrochemical noise), A_{WE} is the steel reaction area, cm^2, and I_{HA} is the corrosion current density obtained from harmonic analysis, in A/cm^2. The PF is an index which varies within 0-1 and is an estimate of the localized attack. PF values are interpreted as follows. PF values < 0.01 suggest generalized corrosion, in the range of 0.01–0.10, generalized corrosion dominates in an intermediate zone, and values > 0.1 imply localized corrosion.

According to Figure 6, in the absence of inhibitors, the PF values decrease as the temperature increases, whereas, at a given temperature, the PF values tendency decreases as the immersion time increases. In all cases, PF values move from the region of generalized corrosion with pitting attack to the region of uniform corrosion. This is expected because the $FeCO_3$ precipitation onto steel surface gives it some protection, and this precipitation is favored by increasing the temperature. However, in the inhibitor's presence, we observed that the PF values are lower as the inhibitor concentration increases in every case (lower values than those observed without presence of inhibitor), reaching values of uniform corrosion. In addition, it was observed that the fluctuations in PF values were higher if the temperature increased. This is possible due to the adsorption-desorption processes of the inhibitor molecules.

3.3. Polarization Curves. Figure 7 shows the polarization curves of API X-70 steel in CO_2-saturated saline solution and different inhibitor concentrations at 30°C, 50°C, and 70°C, respectively. These tests show whether the material under study shows active, passive, or transpassive behavior [26]. In the absence of inhibitor, the tendency of the anodic branch shows that the steel undergoes a continuous dissolution process and that the steel dissolution increases with the test

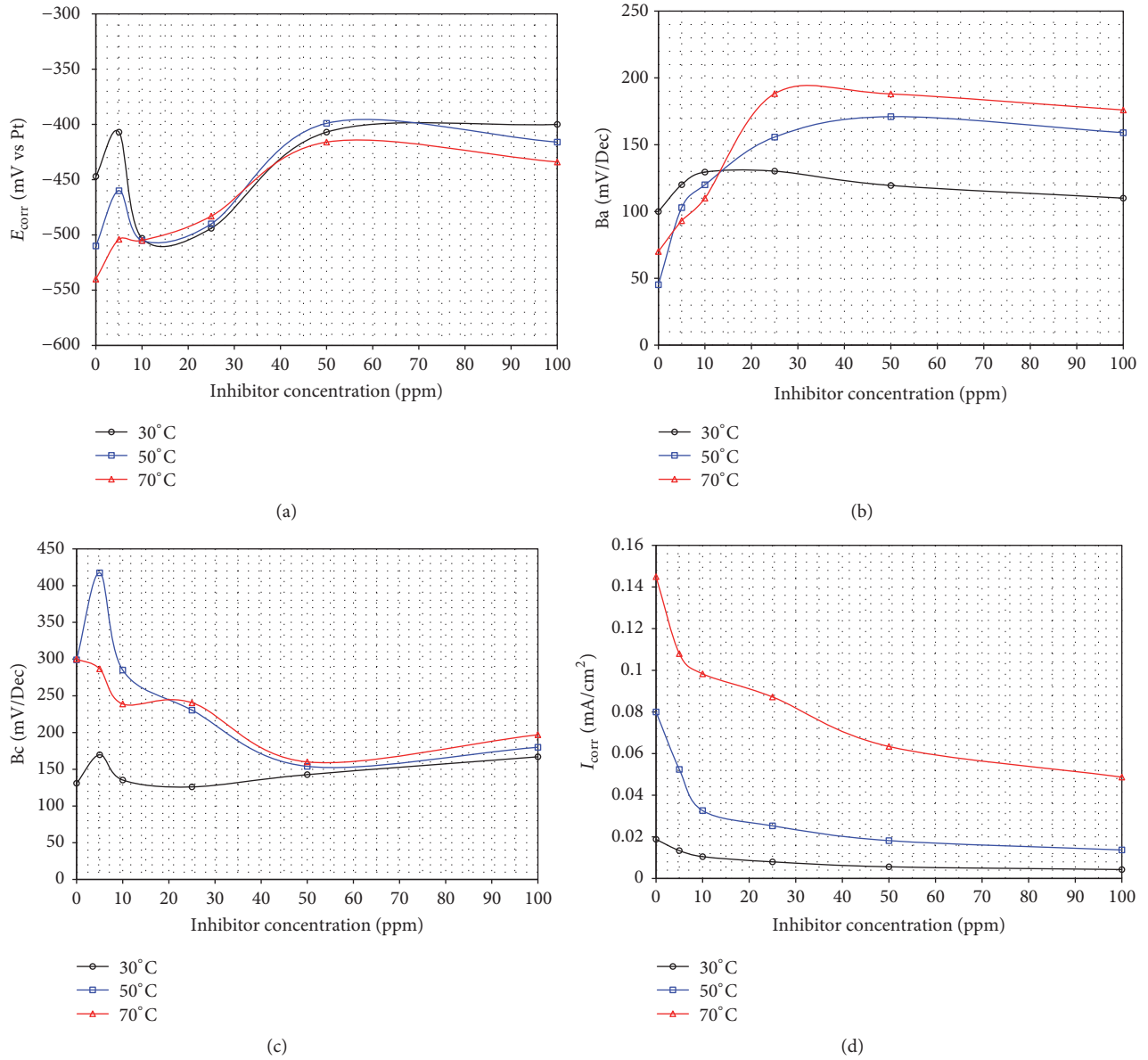

FIGURE 8: Electrochemical parameters for API X-70 steel in CO_2-saturated saline solution as a function of inhibitor concentration and temperature: (a) corrosion potential, (b) anodic slope, (c) cathodic slope, and (d) corrosion current density.

temperature. It has been suggested that the Fe dissolution can occur according to the following reactions [27, 28]:

$$\begin{aligned} \mathrm{Fe} + \mathrm{H_2O} &\longleftrightarrow \mathrm{FeOH_{ads}} + \mathrm{H^+} + \mathrm{e} \\ \mathrm{FeOH_{ads}} &\longrightarrow \mathrm{FeOH^+} + \mathrm{e} \\ \mathrm{FeOH^+} + \mathrm{H^+} &\longleftrightarrow \mathrm{Fe^{2+}} + \mathrm{H_2O} \end{aligned} \quad (10)$$

where the global reaction of anodic dissolution is that represented by (6) [29, 30].

The observed behavior shows that the steel does not have the ability to form a passive layer that protects it from the aggressive environment; that is, its corrosion products are not protective. At temperatures higher than 50°C and longest exposure times, the precipitation of an iron carbonate layer onto steel surface is possible, according to (7). However, the $FeCO_3$ layer offers limited protection due to the presence of imperfections (porosity and cracks), whereby the electrolyte can penetrate and corrode the steel surface causing its detachment [24].

However, when the inhibitor is added, there is an increase in the slope of the anodic branch indicating a decrease in the active behavior, and E_{corr} values move towards nobler values, except at 30°C where, with 10 ppm and 25 ppm of inhibitor, a shift towards more active values was observed. This may be due to the low test temperature which did not facilitate the optimal dispersion of the inhibitor. The dispersion of the inhibitor is favored by increasing the temperature, facilitating its transport towards the metal surface. Similarly, in the presence of the inhibitor, the polarization curves moved towards

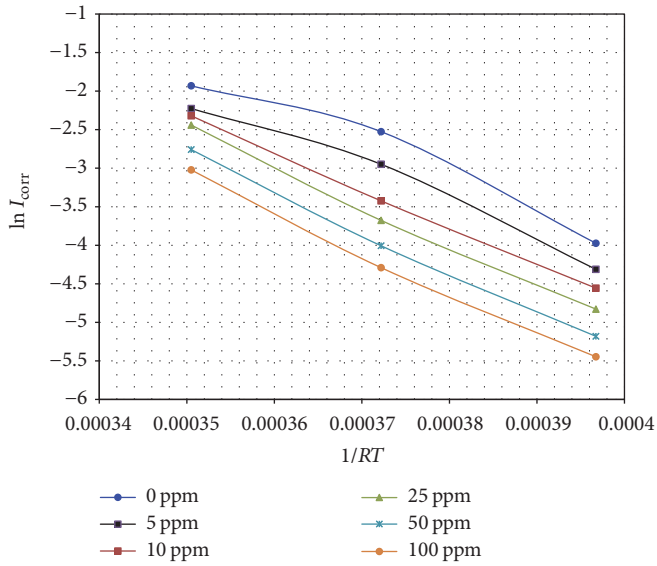

FIGURE 9: $\ln(I_{corr})$ - $1/RT$ relationship for the API X-70 steel evaluated in CO_2-saturated saline solution as a function of the inhibitor concentration.

the lower current density region, indicating a decrease in the corrosion rate of the steel. On the other hand, it is observed that the cathodic branch shows the same shape and trend at all temperatures. This indicates that the reduction reaction is the same, and it is activated thermally, since, by increasing the temperature, the cathodic branch moves to higher current densities. Because the solution is deaerated (continuous bubbling of CO_2, $CO_2 + H_2O = H_2CO_3$), the main possible cathodic reactions are the H^+ ions reduction, the carbonic acid dissociation, and the water reduction [22, 29, 30], according to (2)–(5).

Figure 8 shows the evolution of the electrochemical parameters obtained from Figure 7. It is observed that the tendency of the E_{corr} values (Figure 8(a)) is identical regardless of the test temperature. In general, in presence of the inhibitor, the E_{corr} values are nobler and they tend to increase as a function of the inhibitor concentration. At the same time, E_{corr} values are more active by increasing the temperature; this is because the corrosion phenomenon is a thermally activated process. The tendency in the E_{corr} values allows assuming that the inhibitor evaluated is of the anodic type and that its main action is to suppress the anodic reaction (Fe dissolution). This is supported by the evolution of the anodic slope values (Figure 8(b)) where it is observed that these values are higher than those observed in the absence of inhibitor. Figure 8(c) shows a similar trend in the cathodic slope values; that is, the values increase by increasing temperature. This is congruent with the dissolved CO_2 content. The content of dissolved CO_2 is a function of temperature, solutes concentration, and pressure; that is, increasing the temperature decreases the amount of dissolved CO_2 and therefore increases the cathodic slope. This is a feature of processes controlled by mass transfer [31, 32]. The same occurs with the dissolved O_2 in the solution. In general, at 30°C, the values tend to increase with the inhibitor concentration, and, at higher temperatures, the opposite occurs. Figure 8(d) shows that the steel corrosion rate decreases as the inhibitor concentration increases. This is congruent with the observed from the real-time measurements discussed previously.

The dependence of the metal dissolution rate on temperature can be explained using the Arrhenius equation, where the activation energy of the metal dissolution process can be calculated according to [27]

$$I_{corr} = k \exp\left(-\frac{\Delta E}{RT}\right),$$
$$\ln\left(I_{corr}\right) = \ln k - \frac{\Delta E}{RT}, \tag{11}$$

where ΔE (J mol^{-1}) is the activation energy, which is obtained from the slope of the $\ln(I_{corr})$ versus $1/RT$ relationship, k is a constant, and R is the gas constant (8.314472 J/K-mol). Figure 9 shows the $\ln(I_{corr})$ versus $1/RT$ relationship as a function of inhibitor concentration. The calculated activation energies were 44.5, 45.35, 48.31, 51.55, 52.30, and 52.31 kJ mol^{-1} for 0, 5, 10, 25, 50, and 100 ppm, respectively. This indicates that the anodic reaction is affected by the presence of the inhibitor and that the Fe dissolution rate decreases by increasing the concentration of the inhibitor. In the absence of inhibitor, activation energy values of the order of 14–30 kJ mol^{-1} are reported [27, 33]. Such values are lower than those determined in this study; nevertheless, the fundamental difference is the type of steel evaluated and the NaCl content of the electrolyte.

In order to verify the decrease in Fe dissolution rate, additional experiments based on electrochemical impedance spectroscopy (EIS) measurements were performed. Figure 10 shows the evolution of the EIS spectra as a function of inhibitor concentration after 24 hours of immersion in the electrolyte. From the figure, it is clear that, in the presence of the inhibitor, the magnitude of the capacitive semicircle

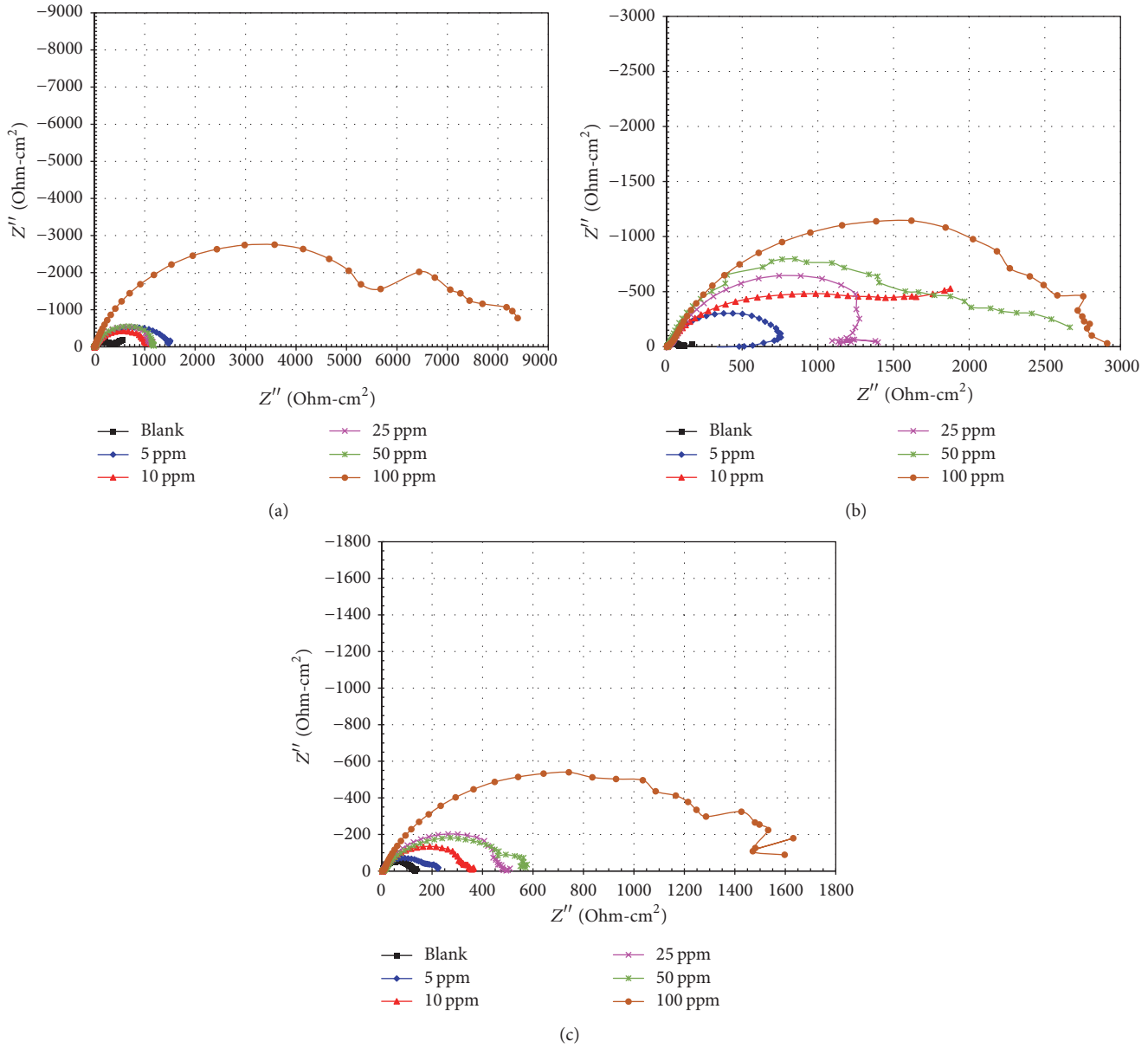

Figure 10: EIS spectra for API X-70 steel in CO_2-saturated saline solution at different concentrations of inhibitor: (a) 30°C, (b) 50°C, and (c) 70°C, after 24 hours of immersion.

increases, and likewise its diameter also increases by increasing the inhibitor concentration. This shows that the charge transfer resistance of the steel increases and consequently decreases its dissolution rate [6, 7].

The fatty amides synthesized from the crude rice bran oil act as corrosion inhibitors, due to the high unsaturation content of their alkyl chains. In short, the inhibitory efficacy was excellent. This allows the adsorption of the inhibitor molecule onto metal surface, thereby decreasing its corrosion rate independently of the test temperature. The above results demonstrate that the use of agroindustrial byproducts (rice bran) is a sustainable source for the synthesis of corrosion inhibitors. Notwithstanding the foregoing in the scientific literature, there are few studies that take into account the byproducts of the rice milling process as an important source for the synthesis of green corrosion inhibitors; for example, the use of the rice husk as raw material for obtaining nanosilicate [34], tannins [35], and momilactone A [36] and the use of rice bran for the extraction of phytic acid have been reported [37–39], and only one study reported the use of rice bran oil for synthesis of fatty acid triazoles [40].

4. Conclusions

Crude rice bran oil is a promising source for the synthesis of bioproducts such as fatty acid amides. The unsaturated fatty acid content of crude rice bran oil makes it an ideal candidate for the synthesis of corrosion inhibitors. The electrochemical

evaluations performed showed that the fatty amides acted as corrosion inhibitors at all test temperatures. In all cases, the inhibition efficiency was at least 95% for the optimum inhibitor concentration. From the real-time measurements, it was observed that, in the presence of the inhibitor, the pitting factor values were lower than those observed in the absence of inhibitor. This is attributed to the adsorption of the inhibitor molecule onto metal surface which prevented the diffusion of the aggressive ions of the electrolyte. Calculation of the activation energy of the corrosion process showed that the inhibitor suppresses the anodic reaction and that this effect increases with the concentration of added inhibitor.

Conflicts of Interest

The authors declare that there are no conflicts of interest regarding the publication of this paper.

Acknowledgments

Financial support from Consejo Nacional de Ciencia y Tecnología (CONACYT, Mexico) (Project 159898) is gratefully acknowledged. E. Reyes-Dorantes and J. Zuñiga-Díaz thank CONACYT, Mexico, for the financial support given to realize their postgraduate studies.

References

[1] M. Heydari and M. Javidi, "Corrosion inhibition and adsorption behaviour of an amido-imidazoline derivative on API 5L X52 steel in CO_2-saturated solution and synergistic effect of iodide ions," *Corrosion Science*, vol. 61, pp. 148–155, 2012.

[2] M. P. Desimone, G. Gordillo, and S. N. Simison, "The effect of temperature and concentration on the corrosion inhibition mechanism of an amphiphilic amido-amine in CO_2 saturated solution," *Corrosion Science*, vol. 53, no. 12, pp. 4033–4043, 2011.

[3] H. M. Abd El-Lateef, V. M. Abbasov, L. I. Aliyeva, E. E. Qasimov, and I. T. Ismayilov, "Inhibition of carbon steel corrosion in CO_2-saturated brine using some newly surfactants based on palm oil: experimental and theoretical investigations," *Materials Chemistry and Physics*, vol. 142, no. 2-3, pp. 502–512, 2013.

[4] P. B. Raja and M. G. Sethuraman, "Natural products as corrosion inhibitor for metals in corrosive media—a review," *Materials Letters*, vol. 62, no. 1, pp. 113–116, 2008.

[5] V. Jovancicevic, S. Ramachandran, and P. Prince, "Inhibition of carbon dioxide corrosion of mild steel by imidazolines and their precursors," *Corrosion*, vol. 55, pp. 449–455, 1999.

[6] J. Porcayo-Calderon, L. M. Martínez De La Escalera, J. Canto, and M. Casales-Diaz, "Imidazoline derivatives based on coffee oil as CO_2 corrosion inhibitor," *International Journal of Electrochemical Science*, vol. 10, pp. 3160–3176, 2015.

[7] J. Porcayo-Calderon, I. Regla, E. Vazquez-Velez et al., "Effect of the unsaturation of the hydrocarbon chain of fatty-amides on the CO_2-corrosion of carbon steel using EIS and real-time corrosion measurement," *Journal of Spectroscopy*, vol. 2015, Article ID 184140, 10 pages, 2015.

[8] M. Lopez, J. Porcayo-Calderon, M. Casales-Diaz et al., "Internal corrosion solution for gathering production gas pipelines involving palm oil amide based corrosion inhibitors," *International Journal of Electrochemical Science*, vol. 10, pp. 7166–7179, 2015.

[9] S. Godavarthi, J. Porcayo-Calderon, M. Casales-Diaz, E. Vazquez-Velez, A. Neri, and L. Martinez-Gomez, "Electrochemical analysis and quantum chemistry of castor oil-based corrosion inhibitors," *Current Analytical Chemistry*, vol. 12, pp. 476–488, 2016.

[10] S. H. Yoo, Y. W. Kim, K. Chung, S. Y. Baik, and J. S. Kim, "Synthesis and corrosion inhibition behavior of imidazoline derivatives based on vegetable oil," *Corrosion Science*, vol. 59, pp. 42–54, 2012.

[11] E. E. Ebenso, U. J. Ekpe, B. I. Ita, O. E. Offiong, and U. J. Ibok, "Effect of molecular structure on the efficiency of amides and thiosemicarbazones used for corrosion inhibition of mild steel in hydrochloric acid," *Materials Chemistry and Physics*, vol. 60, no. 1, pp. 79–90, 1999.

[12] S. Ramachandran, B.-L. Tsai, M. Blanco, H. Chen, Y. Tang, and W. A. Goddard, "Self-assembled monolayer mechanism for corrosion inhibition of iron by imidazolines," *Langmuir*, vol. 12, no. 26, pp. 6419–6428, 1996.

[13] S. Vyas and S. Soni, "Castor oil as corrosion inhibitor for iron in hydrochloric acid," *Oriental Journal of Chemistry*, vol. 27, pp. 1743–1746, 2011.

[14] M. Alam, D. Akram, E. Sharmin, F. Zafar, and S. Ahmad, "Vegetable oil based eco-friendly coating materials: a review article," *Arabian Journal of Chemistry*, vol. 7, no. 4, pp. 469–479, 2014.

[15] L. Canoira, J. García Galeán, R. Alcántara, M. Lapuerta, and R. García-Contreras, "Fatty acid methyl esters (FAMEs) from castor oil: production process assessment and synergistic effects in its properties," *Renewable Energy*, vol. 35, no. 1, pp. 208–217, 2010.

[16] L. A. Rigo, A. R. Pohlmann, S. S. Guterres, and R. C. R. Beck, "Rice bran oil: benefits to health and applications in pharmaceutical formulations," in *Wheat and Rice in Disease Prevention and Health: Benefits, Risks and Mechanisms of Whole Grains in Health Promotion*, R. R. Watson, V. Preedy, and S. Zibadi, Eds., pp. 311–322, Academic Press, 2014.

[17] K. Gul, B. Yousuf, A. K. Singh, P. Singh, and A. A. Wani, "Rice bran: nutritional values and its emerging potential for development of functional food—a review," *Bioactive Carbohydrates and Dietary Fibre*, vol. 6, no. 1, pp. 24–30, 2015.

[18] S. Bhosale and D. Vijayakshmi, "Processing and nutritional composition of rice bran," *Current Research in Nutrition and Food Science*, vol. 3, pp. 74–80, 2015.

[19] D. Kumar, S. M. Kim, and A. Ali, "One step synthesis of fatty acid diethanolamides and methyl esters from triglycerides using sodium doped calcium hydroxide as a nanocrystalline heterogeneous catalyst," *New Journal of Chemistry*, vol. 39, pp. 7097–7104, 2015.

[20] R. D. Kane and S. Campbell, "Real-time corrosion monitoring of steel influenced by microbial activity (SRB) in simulated seawater injection environments," Corrosion/2004, TX: NACE International, Houston, Texas.

[21] D. C. Eden, D. A. Eden, I. G. Winning, and D. Fell, "On-line, real-time optimization of corrosion inhibitors in the field," Corrosion/2006, TX: NACE International, San Diego, California, 12–16 March 2006.

[22] X. Liu, Y. G. Zheng, and P. C. Okafor, "Carbon dioxide corrosion inhibition of N80 carbon steel in single liquid phase and

liquid/particle two-phase flow by hydroxyethyl imidazoline derivatives," *Materials and Corrosion*, vol. 60, no. 7, pp. 507–513, 2009.

[23] F. Farelas, M. Galicia, B. Brown, S. Nesic, and H. Castaneda, "Evolution of dissolution processes at the interface of carbon steel corroding in a CO_2 environment studied by EIS," *Corrosion Science*, vol. 52, no. 2, pp. 509–517, 2010.

[24] S. L. Wu, Z. D. Cui, F. He, Z. Q. Bai, S. L. Zhu, and X. J. Yang, "Characterization of the surface film formed from carbon dioxide corrosion on N80 steel," *Materials Letters*, vol. 58, no. 6, pp. 1076–1081, 2004.

[25] J. Tinnea, B. S. Covino, S. J. Bullard et al., "Electrochemical techniques: investigation of corrosion in a major metropolitan wastewater treatment facility," Corrosion/2004, NACE International, Houston, Texas, March 2004.

[26] B. G. Ateya, F. M. Al Kharafi, and R. M. Abdalla, "Electrochemical behavior of low carbon steel in slightly acidic brines," *Materials Chemistry and Physics*, vol. 78, no. 2, pp. 534–541, 2002.

[27] G. Zhang, C. Chen, M. Lu, C. Chai, and Y. Wu, "Evaluation of inhibition efficiency of an imidazoline derivative in CO_2-containing aqueous solution," *Materials Chemistry and Physics*, vol. 105, no. 2-3, pp. 331–340, 2007.

[28] J. O. Bockris and D. Drazic, "The kinetics of deposition and dissolution of iron: effect of alloying impurities," *Electrochimica Acta*, vol. 7, no. 3, pp. 293–313, 1962.

[29] D. A. López, T. Pérez, and S. N. Simison, "The influence of microstructure and chemical composition of carbon and low alloy steels in CO_2 corrosion. A state-of-the-art appraisal," *Materials and Design*, vol. 24, no. 8, pp. 561–575, 2003.

[30] H. M. Ezuber, "Influence of temperature and thiosulfate on the corrosion behavior of steel in chloride solutions saturated in CO_2," *Materials and Design*, vol. 30, no. 9, pp. 3420–3427, 2009.

[31] X. Liu, P. C. Okafor, and Y. G. Zheng, "The inhibition of CO_2 corrosion of N80 mild steel in single liquid phase and liquid/particle two-phase flow by aminoethyl imidazoline derivatives," *Corrosion Science*, vol. 51, no. 4, pp. 744–751, 2009.

[32] L. M. Rivera-Grau, M. Casales, I. Regla et al., "Effect of organic corrosion inhibitors on the corrosion performance of 1018 carbon steel in 3% NaCl solution," *International Journal of Electrochemical Science*, vol. 8, pp. 2491–2503, 2013.

[33] J. Porcayo-Calderon, L. M. Martínez de la Escalera, J. Canto, M. Casales-Diaz, and V. M. Salinas-Bravo, "Effect of the Temperature on the CO_2-Corrosion of Ni_3Al," in *Proceedings of International Journal of Electrochemical Science*, vol. 10, pp. 3136–3151, 2015.

[34] D. A. Awizar, N. K. Othman, A. Jalar, A. R. Daud, I. A. Rahman, and N. H. Al-Hardan, "Nanosilicate extraction from rice husk ash as green corrosion inhibitor," *International Journal of Electrochemical Science*, vol. 8, pp. 1759–1769, 2013.

[35] K. K. Alaneme, Y. S. Daramola, S. J. Olusegun, and A. S. Afolabi, "Corrosion inhibition and adsorption characteristics of rice husk extracts on mild steel immersed in 1M H_2SO_4 and HCl solutions," *International Journal of Electrochemical Science*, vol. 10, no. 4, pp. 3553–3567, 2015.

[36] M. Prabakaran, S. H. Kim, Y. T. Oh, V. Raj, and I. M. Chung, "Anticorrosion properties of momilactone a isolated from rice hulls," *The Journal of Industrial and Engineering Chemistry*, vol. 45, pp. 380–386, 2017.

[37] H. Sheng, K. Xiaoyang, and F. Chaoyang, "Rice bran extraction used as pickling inhibitor in hydrogen chloride acid," *Journal of the Chinese Society of Corrosion and Protection*, vol. 29, pp. 149–153, 2009.

[38] W. Zhang, H. Gu, L. Xi, Y. Zhang, Y. Hu, and T. Zhang, "Preparation of phytic acid and its characteristics as copper inhibitor," *Energy Procedia*, vol. 17, pp. 1641–1647, 2012.

[39] L. Dong, L. Yuanhua, D. Yigang, and Z. Dezhi, "Corrosion inhibition of carbon steel in hydrochloric acid solution by rice bran extracts," *Anti-Corrosion Methods and Materials*, vol. 58, no. 4, pp. 205–210, 2011.

[40] S. D. Toliwal and K. Jadav, "Fatty acid triazolcs derived from neem, rice bran and karanja oils as corrosion inhibitors for mild steel," *Indian Journal of Chemical Technology*, vol. 16, pp. 32–37, 2009.